



# Osteoblast-derived PTHrP is a potent endogenous bone anabolic agent that modifies the therapeutic efficacy of administered PTH 1–34

Dengshun Miao,<sup>1</sup> Bin He,<sup>2</sup> Yebin Jiang,<sup>3</sup> Tatsuya Kobayashi,<sup>4</sup> Maria A. Sorocéanu,<sup>2</sup> Jenny Zhao,<sup>3</sup> Hanyi Su,<sup>2</sup> Xinkang Tong,<sup>2</sup> Norio Amizuka,<sup>5</sup> Ajay Gupta,<sup>6</sup> Harry K. Genant,<sup>3</sup> Henry M. Kronenberg,<sup>4</sup> David Goltzman,<sup>1</sup> and Andrew C. Karaplis<sup>2</sup>

<sup>1</sup>Calcium Research Laboratory and Department of Medicine, Royal Victoria Hospital of the McGill University Health Centre, and

<sup>2</sup>Division of Endocrinology, Department of Medicine and Lady Davis Institute for Medical Research, Sir Mortimer B. Davis Jewish General Hospital, McGill University, Montréal, Canada. <sup>3</sup>Osteoporosis and Arthritis Research Group, UCSF, San Francisco, California, USA.

<sup>4</sup>Endocrine Unit, Massachusetts General Hospital, Boston, Massachusetts, USA. <sup>5</sup>Division of Oral Anatomy, Department of Oral Biological Sciences, Niigata University, Graduate School of Medical and Dental Sciences, Niigata, Japan. <sup>6</sup>Osta Biotechnologies Inc., Montréal, Canada.

**Mice heterozygous for targeted disruption of *Pthrp* exhibit, by 3 months of age, diminished bone volume and skeletal microarchitectural changes indicative of advanced osteoporosis. Impaired bone formation arising from decreased BM precursor cell recruitment and increased apoptotic death of osteoblastic cells was identified as the underlying mechanism for low bone mass. The osteoporotic phenotype was recapitulated in mice with osteoblast-specific targeted disruption of *Pthrp*, generated using Cre-LoxP technology, and defective bone formation was reaffirmed as the underlying etiology. Daily administration of the 1–34 amino-terminal fragment of parathyroid hormone (PTH 1–34) to *Pthrp*<sup>+/-</sup> mice resulted in profound improvement in all parameters of skeletal microarchitecture, surpassing the improvement observed in treated WT littermates. These findings establish a pivotal role for osteoblast-derived PTH-related protein (PTHrP) as a potent endogenous bone anabolic factor that potentiates bone formation by altering osteoblast recruitment and survival and whose level of expression in the bone microenvironment influences the therapeutic efficacy of exogenous PTH 1–34.**

## Introduction

Osteoporosis is a common disorder characterized by compromised bone strength that predisposes patients to increased fracture risk. It arises, in part, as a consequence of bone loss secondary to an imbalance between the processes of bone resorption and formation during the normal bone remodeling cycle (1). Bone remodeling is necessary for renewal and repair of damaged bone and is mediated by the concerted actions of osteoclasts, which resorb bone, and osteoblasts, which lay down new bone.

A variety of therapeutic modalities are now available for the treatment of osteoporosis (2). Most are antiresorptives that act by inhibiting osteoclast activity, thereby slowing the rate of bone remodeling, but not by rebuilding bone. Agents that rebuild bone are referred to as anabolics. The only bone anabolic agent presently available in the clinical setting is the 1–34 aminoterminal fragment of parathyroid hormone (PTH 1–34). PTH normally regulates serum calcium levels by binding and activating the type 1 PTH receptor (PTHrP) in bone and kidney (3) but also has an in

vivo anabolic role in promoting trabecular bone formation in the fetus (4). When the dose and pattern of administration are carefully selected, exogenous PTH can stimulate bone formation in adult and aged animals of either sex, and in animals with osteopenia induced by disuse, denervation, and immobilization (5). The anabolic action of PTH on cortical and cancellous bone has also been validated in humans (6, 7), and its antifracture efficacy has been established in postmenopausal osteoporotic women (8). At present, however, there is little understanding of the molecular mechanisms that mediate the anabolic effects of PTH. Moreover, significant individual variability exists in the anabolic response to exogenous PTH (9, 10). This has led to the suggestion that the process of PTH-induced bone formation is sensitive to endogenous factors acting in the skeletal microenvironment (10).

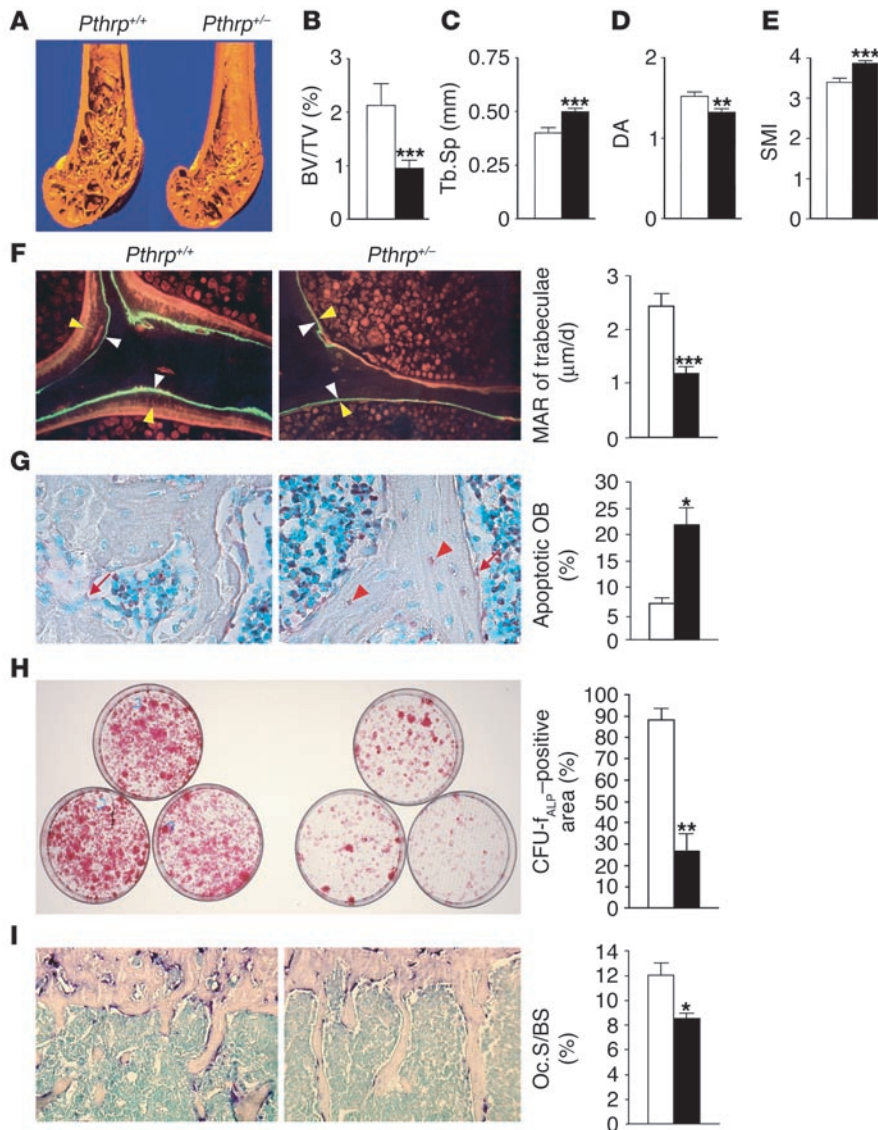
PTH-related protein (PTHrP), a factor isolated from tumors associated with the paraneoplastic syndrome of humoral hypercalcemia of malignancy, shares homology with PTH 1–34 (11–13). As a consequence, this peptide binds and activates PTHrP, which is responsible for mediating the pleiotropic paracrine effects of PTHrP as well as the endocrine actions of PTH on calcium and skeletal homeostasis. Ablation of either PTHrP or PTHrP in mice (14, 15) and humans (16, 17) leads to a form of lethal skeletal dysplasia characterized by decreased proliferation and accelerated differentiation of growth plate chondrocytes.

Osteoblasts are also target cells for locally produced PTHrP and circulating PTH, as these cells express PTHrP and PTHrP (18–22). In previous work, we have shown that 3-month-old

**Nonstandard abbreviations used:** BMD, bone mineral density; BV, bone volume; CFU-f, CFU-fibroblast; CFU-f<sub>ALP</sub>, alkaline phosphatase-positive CFU-f;  $\mu$ CT, micro-CT; HPAP, human placental alkaline phosphatase; MAR, mineral apposition rate; PLP, 2% paraformaldehyde containing 0.075 M lysine and 0.01 M sodium periodate solution; PTH, parathyroid hormone; PTHrP, type 1 PTH receptor; PTHrP, PTH-related protein; TRAP, tartrate-resistant acid phosphatase; TV, tissue volume.

**Conflict of interest:** The authors have declared that no conflict of interest exists.

**Citation for this article:** *J. Clin. Invest.* 115:2402–2411 (2005). doi:10.1172/JCI24918.

**Figure 1**

PTHrP haploinsufficiency causes osteopenia by decreasing bone formation. (A) Three-dimensional reconstruction from CT scans of distal femora from mice at 3 months of age. (B) Quantitative analysis of BV/TV. (C) Trabecular separation (Tb.Sp). (D) Degree of anisotropy (DA). (E) Structure model index (SMI). (F) Calcein (white arrowheads) and tetracycline (yellow arrowheads) labeling of trabecular bone (magnification,  $\times 400$ ). The distance between the 2 labels is used to calculate MAR, shown at right. (G) Red nuclear-stained apoptotic osteoblasts (arrows) and osteocytes (arrowheads) in the trabeculae were detected by TUNEL assay (magnification,  $\times 400$ ). The percentages of apoptotic osteoblasts and osteocytes (Apoptotic OB) are shown at right. (H) Ex vivo cultures of adherent BM cells induced to undergo osteogenic differentiation. Red staining represents alkaline phosphatase enzymatic activity, a marker of osteogenic differentiation. Quantitation of osteogenic colonies is shown at right. (I) TRAP stain for osteoclasts (magnification,  $\times 200$ ) and quantitation of osteoclast surface (Oc.S/BS). Data are shown as the mean  $\pm$  SEM of 6 animals per group. \* $P < 0.05$ ; \*\* $P < 0.01$ ; and \*\*\* $P < 0.001$  for *Pthrp*<sup>+/-</sup> (black bars) versus *Pthrp*<sup>+/+</sup> mice (white bars).

mice heterozygous for the *Pthrp*-null allele (*Pthrp*<sup>+/-</sup> mice) exhibit a form of skeletal haploinsufficiency characterized by decreased bone volume and bony structural alterations consistent with premature, advanced osteoporosis (20). In the *Pthrp*<sup>+/-</sup> haploinsufficiency background, the high bone content observed in *Pth*<sup>-/-</sup> mice (23) is reduced to below WT levels, which indicates that whereas PTH acts to resorb bone for maintenance of calcium homeostasis, PTHrP promotes bone formation (24). Indeed, the anabolic action of administered PTHrP 1–36 on the skeleton has now been documented in women with postmenopausal osteoporosis (25).

Here, we sought to define the underlying etiology for the observed decrease in bone mass in *Pthrp*<sup>+/-</sup> mice, to determine whether osteoblast-derived PTHrP could be a local factor regulating bone formation, and to assess the anabolic efficacy of exogenous PTH 1–34 in the background of PTHrP haploinsufficiency. We demonstrate that the osteoporotic phenotype of the *Pthrp*<sup>+/-</sup> mice arises from defective bone formation due to impaired BM precursor cell recruitment and increased osteoblast/osteocyte apoptosis. Moreover, by generating mice with osteoblast-specific targeted disruption of *Pthrp*, we have

solidified the pivotal role of osteoblast-derived PTHrP in the process of bone formation. We show that osteoblast-derived PTHrP functions as a powerful endogenous bone anabolic agent to promote the recruitment of osteogenic cells and prevent the apoptotic death of osteoblasts and osteocytes. Finally, we report that the anabolic action of administered PTH 1–34 is amplified in the background of *Pthrp* haploinsufficiency, which indicates that the therapeutic efficacy of PTH 1–34 arises in part from modulation of downstream signals in osteogenic cells that are normally regulated by endogenous PTHrP. These findings demonstrate a previously unrecognized capacity of PTHrP produced within the skeletal microenvironment to regulate bone turnover, to potentiate the process of bone formation, and to influence the anabolic properties of administered PTH.

## Results

*Pthrp* haploinsufficiency causes osteopenia by decreasing bone formation. Despite normal serum PTH levels, mice heterozygous for targeted disruption of *Pthrp* (*Pthrp*<sup>+/-</sup> mice) exhibit a form of skeletal haploinsufficiency characterized by decreased *Pthrp* expression in bone

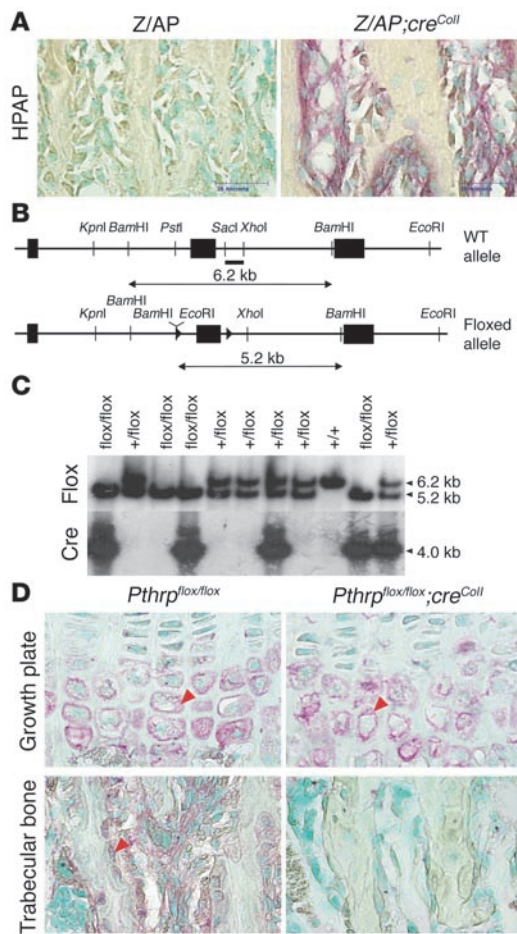


**Figure 2**

Generation of *Pthrp*<sup>flox/flox</sup>; *cre*<sup>Coll</sup> mice. **(A)** Decalcified paraffin sections stained histochemically for HPAP activity. HPAP activity was detected only in preosteoblasts and osteoblasts in Z/AP; *cre*<sup>Coll</sup> mice but not in Z/AP mice. **(B)** Genomic organization of WT and floxed *Pthrp* alleles as well as changes in the restriction enzyme pattern anticipated following digestion of tail-tip genomic DNA with *Bam*HI and hybridization with a 0.65-kb *Sac*I/*Xho*I genomic DNA fragment as probe (–). Arrowheads represent *loxP* sequences flanking exon 3. **(C)** Floxed *Pthrp* allele and *Cre* transgene detected by Southern blot analysis of tail-tip genomic DNA. The flox/flox–*Cre*-positive mice comprised the *Pthrp*<sup>flox/flox</sup>; *cre*<sup>Coll</sup> experimental group, while the *Pthrp*<sup>flox/flox</sup> mice were controls. **(D)** Decalcified paraffin sections immunostained for PTHrP. PTHrP immunoreactivity (red arrowheads) was seen in growth plate chondrocytes of *Pthrp*<sup>flox/flox</sup>; *cre*<sup>Coll</sup> mice and control mice but in preosteoblasts and osteoblasts only in control mice. Magnification, ×400.

To further characterize the cellular mechanisms by which PTHrP promotes bone formation, long bones were stained by TUNEL and apoptotic cells were assessed. In *Pthrp*<sup>+/-</sup> specimens, the number of apoptotic osteoblastic cells was significantly increased (Figure 1G). In addition, BM cells were extracted from WT and heterozygous *Pthrp*-null littermates and plated in culture under conditions promoting osteogenic differentiation. The number of colonies staining positive for alkaline phosphatase, a phenotypic marker of osteoblastic cells, was profoundly reduced in the heterozygous cultures, indicating that recruitment of osteogenic cells was impaired (Figure 1H). These observations provide genetic evidence that normal levels of PTHrP potentiate the recruitment and survival of osteogenic cells and thus are critical for healthy postnatal bone development and maintenance.

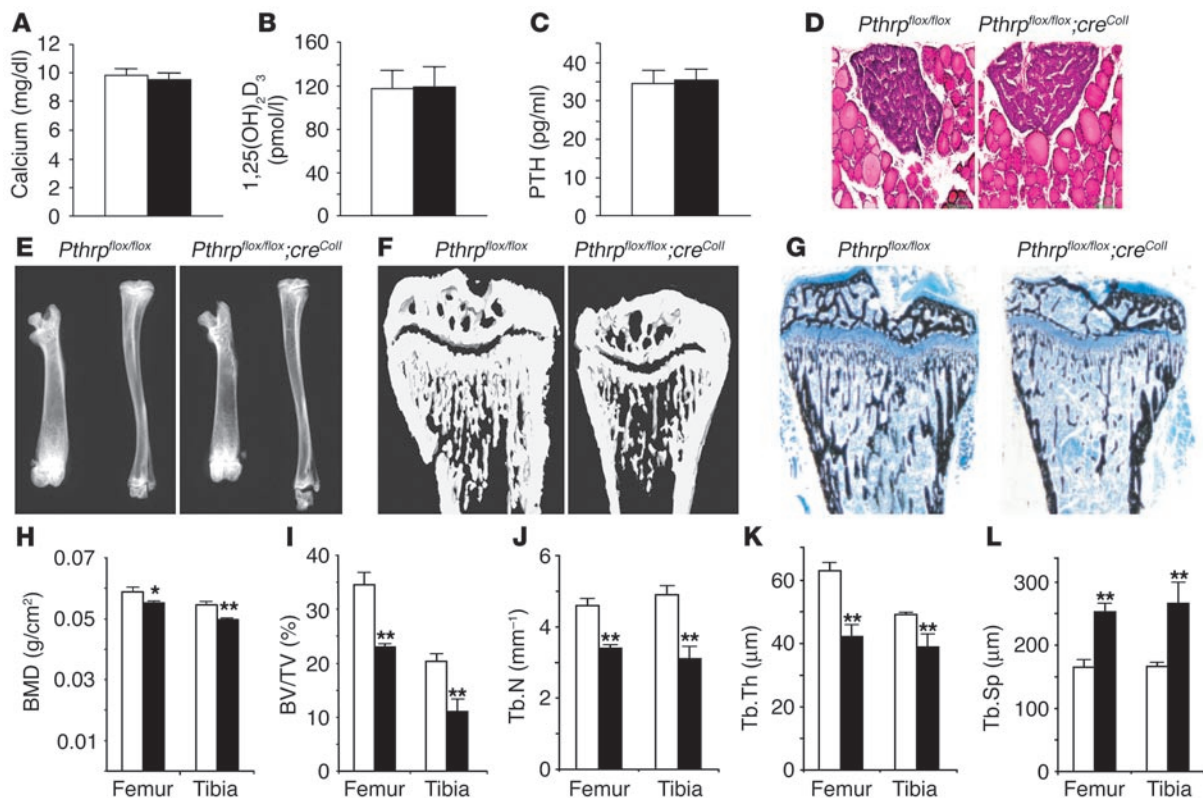
Histomorphometric analysis was also used to determine whether increased osteoclastic activity plays a role in the diminished trabecular bone volume. The tartrate-resistant acid phosphatase–positive (TRAP-positive) osteoclast surface relative to bone surface was in fact reduced in the *Pthrp*<sup>+/-</sup> mice (Figure 1I), thus indicating that increased bone resorption was not responsible for the decreased trabecular bone volume.

*Targeting Pthrp in osteoblasts.* Although PTHrP is expressed in a number of different tissues, previous studies have also documented expression of *Pthrp* and *Pthrp1* mRNA and protein in cells of the osteoblast lineage (15, 20–22). Therefore, it seemed possible that the skeletal consequences of PTHrP haploinsufficiency might reflect the effect of *Pthrp* ablation in osteoblastic cells. Alternatively, in view of the fact that PTHrP has profound effects on cartilage development (15), the observed impairment in bone formation might reflect consequences of diminished *Pthrp* expression in chondrogenic cells that fail to lay down a proper scaffold for normal bone development. Indeed, PTHrP under the control of a collagen II promoter, and therefore selectively expressed in cartilage, did rescue mice expressing the PTHrP-null mutation (26); however, to date, no analysis of the skeletal phenotype has been reported. Therefore, to distinguish between these possibilities and to assess the role of osteoblast-derived PTHrP in normal bone remodeling, an animal model with selective elimination of osteoblastic *Pthrp* was generated.

A transgenic mouse strain in which the *Cre* recombinase was expressed in early osteogenic cells using a modified 2.3-kb fragment of the proximal promoter of the murine pro- $\alpha$ 1(I) collagen gene (*Cre*<sup>Coll</sup>) was first generated. In vivo, these sequences were

and, by 3 months of age, an inappropriate, low trabecular bone volume with increased marrow adiposity (20). This inverse relationship between bone mass and adiposity can be observed in virtually every form of osteopenia. We therefore sought to further characterize the nature of this osteopenic phenotype and delineate the mechanism that leads to it, by examining long bones from these mice and WT littermates using quantitative micro-CT ( $\mu$ CT) and dynamic histomorphometry. At 3 months of age, 3D structure of trabecular bone was significantly altered in the *Pthrp*<sup>+/-</sup> mice compared with *Pthrp*<sup>+/+</sup> littermates and was associated with a 50% decrease in the ratio of bone volume/tissue volume (BV/TV) and increased trabecular separation (Figure 1, A–C). These microarchitectural changes in bone were further substantiated by a decrease in the degree of anisotropy and an increase in the structure model index (Figure 1, D and E). The latter is indicative of the conversion of normal trabecular plates to rodlike structures because of the perforation and loss of connectivity (a consequence of decreased bone formation or increased bone resorption) typically observed in osteoporotic bones.

To determine the mechanism for the observed profound decrease in trabecular bone volume due to PTHrP haploinsufficiency, dynamic histomorphometric analysis was undertaken. There was a marked decrease in the mineral apposition rate (MAR), a parameter of bone formation, in the metaphyseal trabecular bone of heterozygous animals following tetracycline and calcein labeling (Figure 1F). This strongly implicated impaired bone formation as the basis of the osteoporotic phenotype.

**Figure 3**

Osteoblast-specific *Pthrp* ablation reduces BMD and trabecular bone volume. (A–C) Serum calcium (A), 1,25(OH)<sub>2</sub>D<sub>3</sub> (B), and PTH (C) were measured as described in Methods. White bars, *Pthrp<sup>flx/flx</sup>* mice; black bars, *Pthrp<sup>flx/flx</sup>;cre<sup>Coll</sup>* mice. Data are shown as mean ± SEM. (D) Parathyroid gland histology was assessed from paraffin sections of thyroparathyroidal tissue stained with H&E. Magnification, ×200. (E) Faxitron radiographs of femur and tibia. (F) Three-dimensional reconstruction of the proximal tibiae from μCT scans. (G) Micrographs from undecalcified sections of the proximal end of tibia stained with the von Kossa procedure. Magnification, ×25. (H) BMD measurements at femurs and tibiae. (I–L) Quantitative histomorphometry for BV/TV (I), trabecular number (Tb.N) (J), trabecular thickness (Tb.Th) (K), and trabecular separation (L). Data shown represent mean ± SEM of 5–6 animals per group. \**P* < 0.05 and \*\**P* < 0.01 for *Pthrp<sup>flx/flx</sup>;cre<sup>Coll</sup>* (black bars) versus *Pthrp<sup>flx/flx</sup>* control mice (white bars).

reported to confer nearly exclusive specificity of expression of the transgene in osteoblasts (27). This was confirmed here when the *Cre<sup>Coll</sup>* transgenic mice were crossed with double-reporter Z/AP mice (28), which provide a convenient and reliable readout of Cre recombinase activity. Cre activity successfully removed the *lacZ* gene in cells of the osteogenic lineage, allowing expression of the second reporter, the human placental *Alkaline Phosphatase* (HPAP) gene (Figure 2A). Other tissues failed to express Cre and did not stain for HPAP enzymatic activity.

*Pthrp* targeting centered on the scheme used to generate *Pthrp<sup>-/-</sup>* mice, in which 1.2 kb of endogenous sequence (*PstI/SacI* fragment) containing exon 3 of the murine gene resulted in a null allele (Figure 2B) (14). Matings between mice homozygous for a “floxed” *Pthrp* allele, i.e., exon 3 flanked by 2 *loxP* sites (*Pthrp<sup>flx/flx</sup>* mice) (27), and *Cre<sup>Coll</sup>* transgenic mice, gave rise to *Pthrp<sup>flx/flx</sup>* animals carrying the *Cre<sup>Coll</sup>* transgene (*Pthrp<sup>flx/flx</sup>;cre<sup>Coll</sup>* mice) (Figure 2C). The nearly complete absence of PTHrP expression in osteoblasts and osteocytes due to Cre recombinase excisional activity was demonstrated by lack of immunostaining in these cells, while PTHrP immunoreactivity was preserved in growth plate chondrocytes (Figure 2D). These findings confirmed the extensive and highly specific excision of *Pthrp* from cells of the osteoblastic lineage.

*Pthrp<sup>flx/flx</sup>;cre<sup>Coll</sup>* mice grew normally and weighed the same as control *Pthrp<sup>flx/flx</sup>* littermates (data not shown). Analysis at 6 weeks of age demonstrated normal total serum calcium, 1,25(OH)<sub>2</sub>D<sub>3</sub>, and PTH levels relative to control mice (Figure 3, A–C). Moreover, histological assessment of parathyroid glands did not reveal any size difference between the 2 groups (Figure 3D).

*Reduced bone mineral density and trabecular bone volume in Pthrp<sup>flx/flx</sup>;cre<sup>Coll</sup> mice.* Radiographic evaluation of the long bones was undertaken at 6 weeks of age. The *Pthrp<sup>flx/flx</sup>;cre<sup>Coll</sup>* specimens, although of the appropriate shape and size, differed from *Pthrp<sup>flx/flx</sup>* bones from sex-matched littermates by being less radiopaque (Figure 3E), suggesting the presence of osteopenia. This was further verified by 3D μCT scanning and histological analysis of mutant long bones, which demonstrated a pronounced increase in marrow space with scattered thin spicules of trabecular bone (Figure 3, F and G). Bone mineral density (BMD), as measured by dual-energy x-ray absorptiometry, was decreased in *Pthrp<sup>flx/flx</sup>;cre<sup>Coll</sup>* bone specimens (Figure 3H). Trabecular bone volume quantified at the distal femur and proximal tibia was reduced (Figure 3I), and trabecular number and thickness were decreased, whereas trabecular separation was increased (Figure 3, J–L). However, there was no corresponding increase in BM adiposity, as observed in the *Pthrp<sup>-/-</sup>* mice.

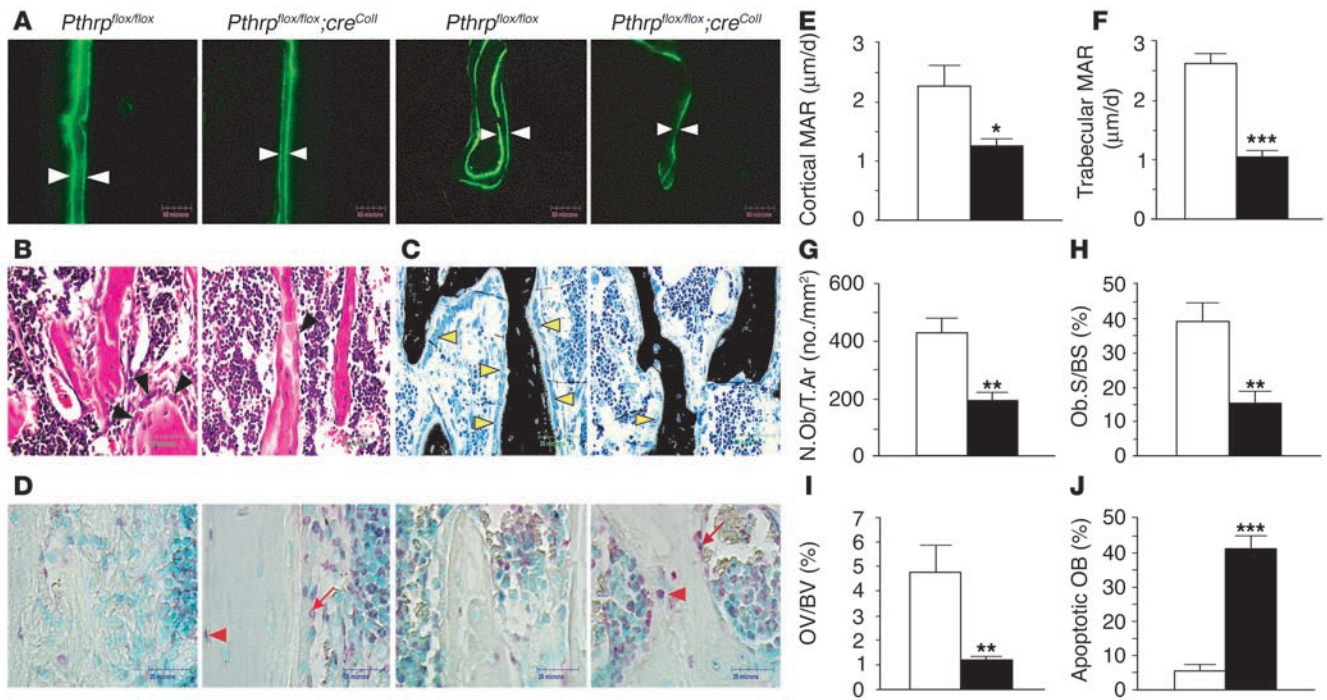


**Figure 4** Impaired osteoblastic bone formation in the absence of osteoblast-derived PTHrP. (A) Micrographs of the proximal ends of tibiae after double calcein labeling of the cortex (left 2 panels) and trabeculae (right 2 panels). (B) Micrographs from decalcified paraffin sections stained with H&E. Black arrowheads show osteoblastic cells. (C) Micrographs from undecalcified sections stained by the von Kossa procedure. White arrowheads show osteoids. (D) Red nuclear-stained apoptotic osteoblasts (arrows) and osteocytes (arrowheads) in the endosteum (left 2 panels) and trabeculae (right 2 panels) were detected by TUNEL assay. (E–J) Quantitative assessment by histomorphometric analysis of MAR at the cortex (E), MAR at trabeculae (F), osteoblast number/tissue area ratio (N.Ob/T.Ar) (G), osteoblast volume/bone surface ratio (Ob.S/BS) (H), osteoid volume/bone volume ratio (OV/BV) (I), and percentage of apoptotic osteoblasts (J). Data shown represent mean ± SEM of 5–6 animals per group. \**P* < 0.05, \*\**P* < 0.01, and \*\*\**P* < 0.001 for *Pthrp<sup>flax/flax;creColl</sup>* (black bars) versus *Pthrp<sup>flax/flax</sup>* mice (white bars).

*Reduced osteoblastic bone formation in Pthrp<sup>flax/flax;creColl</sup> mice.* To elucidate the mechanism that underlies the observed decrease in bone volume in the *Pthrp<sup>flax/flax;creColl</sup>* mice, we sought to determine whether these osteoporotic changes were a consequence of impaired bone formation. Following in vivo double calcein labeling of bones, MAR, a measure of bone formation, was assessed ex vivo in cortical and trabecular bone. MAR was reduced by 45% and 60% in the tibial cortex and trabeculae, respectively, of *Pthrp<sup>flax/flax;creColl</sup>* mice compared with control littermates (Figure 4, A, E, and F).

Assessment of osteoblast number and function using histological and static histomorphometric analysis was then undertaken. A marked reduction in osteoblast number and osteoid volume was seen in mutant long bone sections (Figure 4, B, C, and G–I). Thus, osteoblast number and surface were decreased by 55% and 60%, respectively, while osteoid volume was reduced by 75% in the *Pthrp<sup>flax/flax;creColl</sup>* bone specimens.

*Increased osteoblast apoptosis in Pthrp<sup>flax/flax;creColl</sup> mice.* We then sought to identify the mechanisms by which osteoblast number and function are altered in the absence of PTHrP. Using TUNEL assay, we observed that in the absence of osteoblast-derived PTHrP, the percentage of apoptotic osteoblasts/osteocytes in *Pthrp<sup>flax/flax;creColl</sup>* bones increased more than 8-fold compared with that in controls (Figure 4, D and J). Therefore, osteoblast-derived PTHrP influences bone formation, at least in part, by maintaining osteoblast/osteocyte survival.

*PTHrP promotes BM stem cell commitment to osteogenic lineage.* To elucidate whether the observed decrease in osteogenic cell commitment observed in ex vivo BM cultures from *Pthrp<sup>+/-</sup>* mice was due to its relative absence from osteoblastic cells rather than from surrounding marrow-derived cells, similar studies were performed using BM cultures derived from control and *Pthrp<sup>flax/flax;creColl</sup>* mice. Compared with controls, *Pthrp<sup>flax/flax;creColl</sup>* cultures repeatedly demonstrated a marked impairment (~45%) in their capacity to differentiate to CFU-fibroblast (CFU-f) and alkaline phosphatase-positive CFU-f (CFU-f<sub>ALP</sub>) colonies (Figure 5, A and B). Therefore, PTHrP exerts additional beneficial effects on bone formation by potentiating the osteogenic lineage from BM precursors.

To determine whether these osteoporotic changes were a consequence of increased osteoclastic bone resorption in the *Pthrp<sup>flax/flax;creColl</sup>* mice, we also assessed parameters of osteoclastic bone resorption. The number and size of TRAP-positive osteoclasts were decreased in the mutant bones compared with controls (Figure 5C). Histomorphometric analysis confirmed a decrease in osteoclast number (43%) and osteoclast surface (52%) in the *Pthrp<sup>flax/flax;creColl</sup>* mice (Figure 5, D and E), indicating that the observed decrease in bone volume was not due to increased bone resorption.

*PTH and PTHrP interaction at the level of the osteoblasts.* Next, we sought to examine whether the anabolic action of exogenously administered PTH 1–34 might be modified in the setting of PTHrP haploinsufficiency. Three-month-old *Pthrp<sup>+/-</sup>* male mice

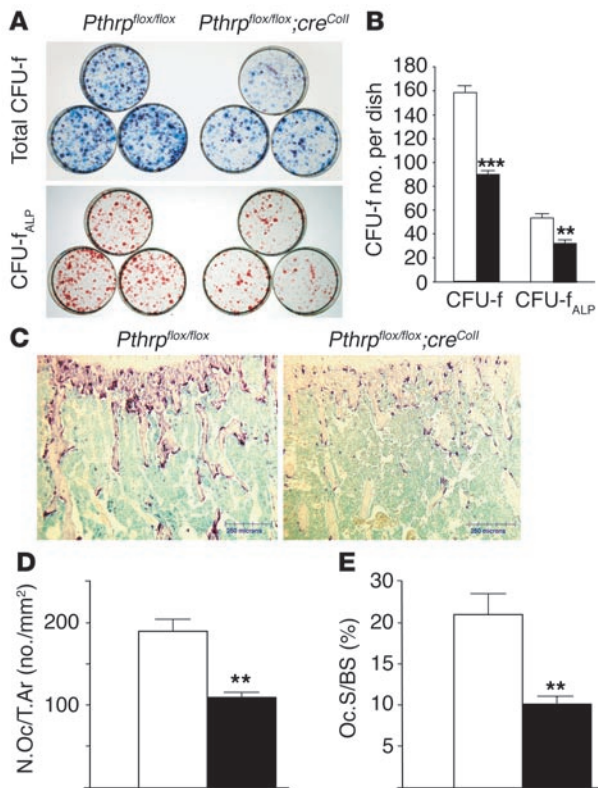


**Figure 5**

Formation of osteogenic colonies and osteoclasts in the absence of osteoblast-derived PTHrP. (A) Ex vivo primary BM cell cultures stained with methyl blue (top panels) or cytochemically for alkaline phosphatase (bottom panels). (B) Positive CFU-f and CFU-f<sub>ALP</sub> numbers were counted manually and are presented as mean ± SEM of 3 animals per group. The experiment was performed twice with similar results. (C) Bone sections stained histochemically for TRAP activity. (D and E) Quantitative assessment by histomorphometric analysis of osteoclast number/total area ratio (N.Oc/T.Ar) (D) and osteoclast surface (E). Data shown represent mean ± SEM of 5–6 animals per group. \*\**P* < 0.01 and \*\*\**P* < 0.001 for *Pthrp*<sup>flx/flx;cre<sup>Coll</sup></sup> (black bars) versus *Pthrp*<sup>flx/flx</sup> mice (white bars).

ber (24% vs. -4%), thickness (55% vs. 12%), connectivity (306% vs. 37%), and degree of anisotropy (9% vs. -6%) were increased, while trabecular spacing (-22% vs. 3%) and structure model index (-32% vs. -1%) were decreased in specimens from PTHrP-haploinsufficient mice (Figure 7, A–G). Similar anabolic effects of PTH 1–34 were observed in cortical bone, where thickness increased significantly (Figure 7H).

**Discussion**

Studies with the *Pth*<sup>-/-</sup>*Pthrp*<sup>+/-</sup> double mutants have suggested that in the adult animal the main action of endogenous PTH is to resorb bone and maintain calcium homeostasis while locally produced PTHrP acts to promote bone formation (24). Here we confirm, using further genetic analyses, that, despite normal serum levels of circulating PTH, it is PTHrP deficiency at the level

and WT male littermates were injected s.c. with either vehicle or human PTH 1–34 (40 µg/kg/d) for 3 months, at which time µCT analysis of the skeleton was undertaken. In WT bones, administered PTH 1–34 had modest positive effects on all parameters examined. In contrast, profound anabolic changes were observed in treated bone specimens from *Pthrp*<sup>+/-</sup> mice (Figure 6, A and B). The pronounced anabolic effect of PTH 1–34 on the mutant bones was also apparent following double calcein labeling (Figure 6C). The distance between the 2 labels permitted calculation of the MAR, which is indicative of the bone formation rate, and MAR was significantly increased compared with that in control littermates (Figure 6D). Similar findings were observed with PTH 1–34 in *Pthrp*<sup>flx/flx;cre<sup>Coll</sup></sup> mice (data not shown).

Dynamic histomorphometry and µCT analysis of long bones were used to quantify the anabolic alterations associated with PTH 1–34 administration (Figure 7). BV/TV, a parameter very similar to volumetric trabecular BMD, was increased 178% from the level in vehicle-treated *Pthrp*<sup>+/-</sup> mice, compared with 19% from the level in vehicle-treated WT mice. Similarly, trabecular num-

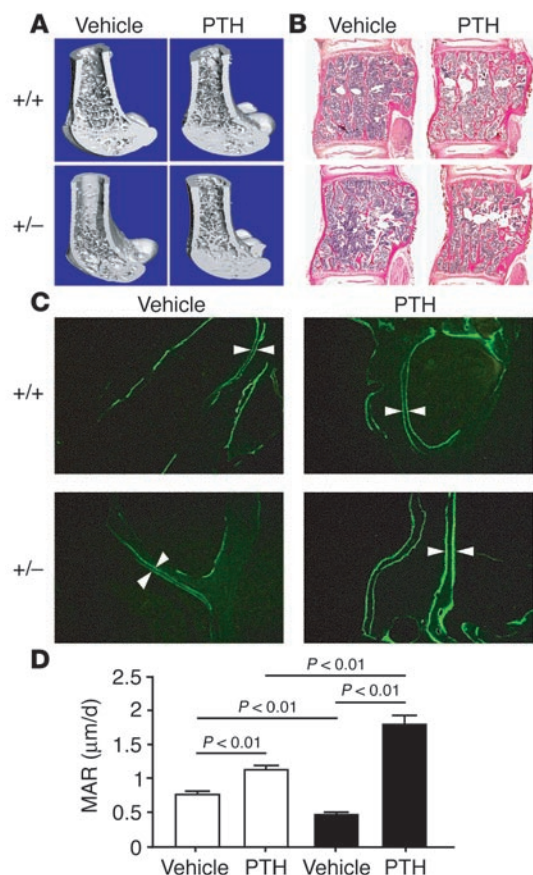


**Figure 6**

Anabolic action of PTH 1–34 in *Pthrp*<sup>+/+</sup> and *Pthrp*<sup>+/-</sup> mice. (A) Three-dimensional reconstruction of the distal femora from µCT scans after treatment with either vehicle (left panels) or PTH 1–34 (40 µg/kg/d) (right panels). (B) Micrographs of decalcified paraffin sections of vertebrae stained with H&E after treatment with either vehicle (left panels) or PTH 1–34 (right panels). Magnification, ×25. (C) Histomorphometric examination of double calcein labeling after treatment with either vehicle (left panels) or PTH 1–34 (right panels). Magnification, ×400. (D) Quantitative assessment of MAR. White bars, *Pthrp*<sup>+/+</sup> mice; black bars, *Pthrp*<sup>+/-</sup> mice.

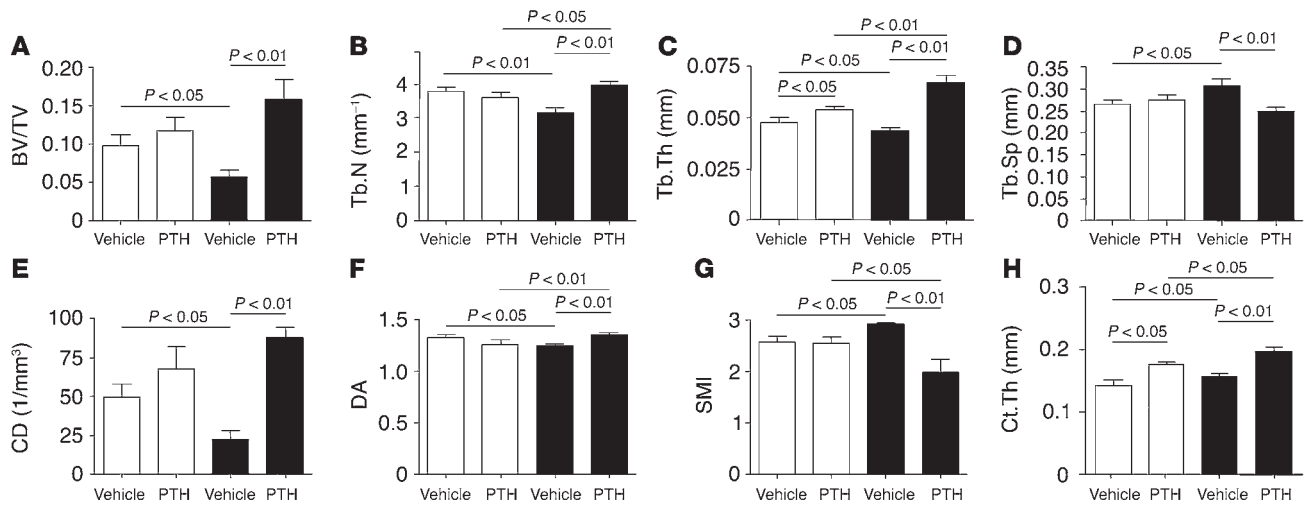


**Figure 7** Data from quantitative assessment. (A) BV/TV. (B) Trabecular number. (C) Trabecular thickness. (D) Trabecular separation. (E) Trabecular connectivity (CD). (F) Degree of anisotropy. (G) Structure model index. (H) Cortical thickness (Ct.Th). Data shown represent mean ± SEM of 5–7 animals per group. White bars, *Pthrp*<sup>+/+</sup> mice; black bars, *Pthrp*<sup>+/-</sup> mice.

of the bone microenvironment, and specifically in osteogenic cells, that leads to the profound osteoporotic phenotype of the *Pthrp*<sup>+/-</sup> and *Pthrp*<sup>flx/flx;creCol1</sup> mice. The generation and analysis of these mutant mice have therefore identified osteoblast-derived PTHrP as a potent endogenous bone anabolic agent that modulates osteogenic cell recruitment and the apoptotic death of osteoblasts and osteocytes. Endogenous PTHrP concentrations also influence the therapeutic efficacy of exogenously administered PTH 1–34.

It has been proposed that in the early stages of osteogenic cell lineage development, PTHrP expressed within the skeletal microenvironment likely functions as a signal to regulate determination of cell fate. Since the same pluripotent stromal cells in the BM compartment can give rise to adipocytes and osteoprogenitor cells (28), the increased adiposity and concomitant osteopenia in the *Pthrp*<sup>+/-</sup> mice could be attributed to altered stem cell differentiation as a consequence of PTHrP haploinsufficiency. In previous studies we have shown that PTHrP signaling in preadipocytes by protein kinase A enhances MAPK activity, which leads to phosphorylation of PPARγ, the master regulator of adipocyte differentiation, and hence repression of the adipogenic differentiation program (29). We also demonstrated in an in vitro cell model that PTHrP can be a potent inhibitor of adipocytic differentiation and a powerful inducer of osteogenic differentiation from pluripotent mesenchymal stem cells by modifying the activity of bone morphogenetic protein-2 (30). Consequently, if signals for determination of cell fate were altered by decreased local concentrations of PTHrP in vivo, it would be predicted that pluripotent BM stem cells would favor the adipocytic differentiation program, leading to the concomitant reduction in osteogenic cells. This premise was corroborated here in vivo by the osteoporotic phenotype and associated increased BM adiposity in the *Pthrp*<sup>+/-</sup> mice (20). In contrast, increased marrow adiposity was absent in the *Pthrp*<sup>flx/flx;creCol1</sup> long bones. This may be due to the timing of *Pthrp* ablation relative to the osteogenic differentiation program. Expression of Cre recombinase by the modified *Col1a1* promoter may take place at a time when commitment to the osteogenic program has already been made and therefore the shift to the adipocytic program would not

occur. In the *Pthrp*<sup>+/-</sup> mice, the relative absence of PTHrP occurs much earlier in the cell commitment program, affecting both osteogenic and adipocytic lineages and thereby leading to the concomitant potentiation of adipocytic cell differentiation.

The observation from the present work that relative or complete absence of osteoblast-derived PTHrP leads to the apoptotic death of osteoblasts and osteocytes provides an additional mechanistic explanation for the profound osteopenia in the *Pthrp*<sup>+/-</sup> and *Pthrp*<sup>flx/flx;creCol1</sup> mice. The antiapoptotic properties of PTHrP have been observed in a variety of cell types (20, 31–37). While the molecular mechanisms by which PTHrP signaling in the osteoblast prevents apoptotic cell death remain to be determined, a number of them may be operative. These include paracrine/autocrine actions involving upregulation of *Bcl2* expression (32) as well as intracrine mechanisms (31, 34, 35) via modulation of ribosome synthesis (38), or interaction of the internalized receptor with 14-3-3 proteins (39), a family of phosphoserine/phosphothreonine-binding molecules suggested to support cell survival.

PTH and PTHrP are known to regulate osteoclastic differentiation and function via the RANK/RANK ligand system (40). Our finding that reduction of osteoblast-derived PTHrP in *Pthrp*<sup>+/-</sup> and *Pthrp*<sup>flx/flx;creCol1</sup> mice decreases osteoclast number and activity identifies locally produced PTHrP as a regulator of bone turnover. In contrast to PTH deficiency, however, which is associated, in the adult animal, with reduced bone turnover and net bone accrual (23), deficiency of osteoblastic PTHrP results in reduced bone turnover with net bone loss. This emphasizes the unique role osteoblast-derived PTHrP plays in bone anabolism. Future studies will be required to assess which factors modulate osteoblast PTHrP expression in physiological and pathophysiological states.

In the present work we also provide evidence that the levels of osteoblast expression of PTHrP may be relevant to the observed anabolic effect of daily-administered PTH 1–34. We show that the anabolic benefit of PTH is more pronounced in *Pthrp*<sup>+/-</sup> mice and surpasses that in treated WT animals. To date, little is known about how these related proteins interact to modulate bone cell function. Both exert most if not all cellular effects by binding



of their N-terminal region to the common G protein-coupled PTHR1 on target cells. It is possible that decreased receptor occupancy by the endogenous PTHrP ligand (haploinsufficiency and complete absence) would provide for increased receptor availability for intermittent activation by administered PTH 1–34, leading to net bone formation. It is also possible that altered kinetics of receptor activation and desensitization determine the interaction of the 2 peptides. In this scenario, local production of PTHrP derived from cells of the osteoblast phenotype could rapidly attenuate cell surface PTHR1 expression in osteoblastic cells and thereby reduce responsiveness to administered PTH. Indeed, rat ROS 17/2.8 osteoblastic cells overexpressing full-length PTHrP cDNA exhibit a marked decrease in the expression of *PTHrP* mRNA and PTHrP ligand binding, as well as a corresponding decrease in PTH- and PTHrP-stimulated cAMP response (41).

We previously reported that in PTH-deficient (*PTH*<sup>-/-</sup>) mice, PTHrP levels were slightly increased in bone (24). Whether this effect of the absence of PTH is direct or indirect, e.g., by altering 1,25(OH)<sub>2</sub>D<sub>3</sub> levels in vivo, is unclear (24). Nevertheless, it is possible therefore that PTH administration could reduce skeletal PTHrP concentrations. This would enhance the effect of administered PTH either by allowing more effective competition for receptor occupancy or by altering receptor numbers. An initial reduction of osseous PTHrP, as in *Pthrp*<sup>+/-</sup> mice, could then produce an amplification of this effect of administered PTH.

Desensitization of the majority of G protein-coupled receptors is mediated by the binding of arrestins. In keeping with this mechanism, binding of PTHrP to PTHR1 would trigger internalization of a  $\beta$ -arrestin-mediated complex, and receptor sequestration would occur in a dynamin- and clathrin-dependent manner (42). Hence, normal concentrations of PTHrP in bone would tend to facilitate PTHR1 desensitization and internalization at the level of the osteoblast. On the other hand, osteoblast cell surface expression of the common receptor and hence its potential availability for intermittent downstream anabolic signaling would be increased when PTHrP levels were diminished, as we showed here in *Pthrp*<sup>+/-</sup> long bones. Indeed, recent data indicate that pharmacological manipulation of G protein receptor kinase (GRK) activity in bone promotes osteogenesis (43). Hence, targeted expression of a GRK inhibitor to mature osteoblasts using the osteocalcin gene 2 (*OG2*) promoter was associated with enhanced PTHR1-stimulated cAMP generation, diminished agonist-induced phosphorylation of the receptor, and a predominantly anabolic effect in vivo, consistent with attenuation of receptor desensitization.

The results here also bear relevance to the clinical setting. Analyses of randomized, placebo-controlled trials with PTH have uncovered variability in the skeletal response to PTH whereby some recipients are nonresponders but others have a marked anabolic response (9, 10). The reason for such individual differences in PTH responsiveness remains unclear. Because such variation in response was not observed with the anti-resorptive drugs, it was suggested that the anabolic component of bone remodeling is sensitive to endogenous growth factors that contribute to this heterogeneous response to PTH action (10). Our findings have now identified PTHrP as one such pivotal modulator of the osseous anabolic action of PTH. However, in contrast to other potential factors such as IGF-1 (44, 45) and FGF-2 (46, 47), whose absence diminishes the anabolic response to PTH 1–34, PTHrP is a factor whose insufficiency in fact accentuates the anabolic action

of administered PTH. Extrapolating our findings to the clinical setting, variability in skeletal concentrations of PTHrP as a result of heritable or environmental determinants could impact responsiveness of patients to daily PTH 1–34. Downstream modulators such as PTHrP may therefore help to predict the clinical efficacy of pharmacologically administered PTH and enhance its specificity for treating this debilitating disorder.

## Methods

**Generation of transgenic and knockout mice.** A *Cre* expression vector constructed in pOG44 (Stratagene) was a gift from S. O’Gorman (Salk Institute for Biological Studies, La Jolla, California, USA). A 2.3-kb fragment of the murine pro- $\alpha 1(I)$  collagen gene promoter was excised from pJ251 LacZ expression vector using *SacII* and *BamHI*. This DNA fragment was ligated to the *SacII*/*BglII* fragment of the *Cre* expression vector to replace the *CMV* promoter with the pro- $\alpha 1(I)$  collagen promoter. The insert was released from the vector by digestion with *SacII* and *SalI* and was subjected to pronuclear injection using fertilized eggs from FVB/N mice. Ten founder lines were screened by in situ hybridization for *Cre* mRNA in neonatal tibiae. One line was selected based on its robust and specific *Cre* expression in osteoblasts (*cre*<sup>coll</sup>). This line was further examined using Rosa 26-R reporter mice and was confirmed for its specific and efficient *Cre* activity.

*Z/AP;cre*<sup>coll</sup> mice were generated by crossing of *Z/AP* reporter mice (provided by C. Lope, Sunnybrook Health Science Centre, Toronto, Ontario, Canada), which express  $\beta$ -gal in the absence of *Cre* but HPAP in its presence, with mice expressing *cre* driven by the 2.3-kb murine pro- $\alpha 1(I)$  collagen gene promoter (*cre*<sup>coll</sup> mice).

To generate mice with osteoblasts lacking *Pthrp* (*Pthrp*<sup>flax/flax;cre</sup><sup>coll</sup> mice), *Pthrp*<sup>+/-flax</sup> mice (with exon 3 of *Pthrp* flanked by *loxP* sites) carrying the *Cre* recombinase transgene under the control of the 2.3-kb fragment of the murine pro- $\alpha 1(I)$  collagen gene promoter (*coll*) were crossed with mice homozygous for the floxed *Pthrp* allele (27). To genotype mice, floxed *Pthrp* and *Cre* were detected by Southern blot analysis of tail-tip genomic DNA, as previously described (27).

**Serum biochemistry.** Serum calcium and phosphorus were determined by autoanalyzer (Beckman Synchron 67; Beckman Coulter). Serum intact PTH and 1,25(OH)<sub>2</sub>D<sub>3</sub> determinations were performed using commercially available ELISA (Immutopics Inc.) and RIA (Immunodiagnostic Systems Ltd.) kits, respectively.

**Radiography and measurement of BMD.** For radiography, femurs and tibiae were removed and dissected free of soft tissue, and x-ray images were taken with a Faxitron (model 805; Faxitron X-Ray Corp.), under constant conditions (22 kV, 4 minutes’ exposure), using Kodak X-Omat TL film (Eastman Kodak Co.). For measurement of femoral and tibial BMD, a PIXImus densitometer (Lunar PIXImus Corp.) was used (5-minute image acquisition with the precision of 1% coefficient of variation for skeletal BMD). The PIXImus software automatically calculated the BMD and recorded the data in Microsoft Excel files (Microsoft Corp.).

**Histology.** All animal studies were approved by the Animal Care Committee of McGill University. Six-week-old mice were sacrificed, and tissues were removed and fixed in PLP fixative (2% paraformaldehyde containing 0.075 M lysine and 0.01 M sodium periodate solution) overnight at 5°C and processed histologically (23). Briefly, the distal end of femurs and the proximal end of tibiae were decalcified in EDTA glycerol solution for 5–7 days at 5°C. After paraffin embedding, 5- $\mu$ m sections were cut on a rotary microtome. The sections were stained with H&E, and histochemically for HPAP and TRAP activity. Undecalcified distal ends of femurs were embedded in LR White acrylic resin (London Resin Co.). One-micrometer sections were cut on an ultramicrotome, stained for mineral with the von Kossa staining procedure, and counterstained with toluidine blue.



**HPAP staining.** Tissue staining for HPAP activity was performed as previously described (27, 48). Histochemical staining for TRAP was conducted as previously described (23). For PTHrP immunohistochemistry, paraffin sections were stained for PTHrP using the avidin-biotin-peroxidase complex technique. For detection of apoptotic cells, dewaxed paraffin sections were stained with an In Situ Cell Death Detection Kit (Roche Diagnostics Corp.) (4).

**PTHrP immunohistochemistry.** Paraffin sections were stained for PTHrP using the avidin-biotin-peroxidase complex technique as described previously (4).

**Detection of apoptotic cells.** Dewaxed paraffin sections were stained with an In Situ Cell Death Detection Kit (Roche Diagnostics Corp.) using a previously described protocol (4). Briefly, after treatment with 3 µg/ml of proteinase K for 20 minutes at room temperature, the sections were incubated with a reaction mixture for TUNEL of DNA strand breaks for 60 minutes at 37°C. Sections were then incubated with Converter-AP (Sigma-Aldrich) for 30 minutes at 37°C, and alkaline phosphatase was visualized after 10–15 minutes of treatment with Fast Red TR/Naphthol AS-MX phosphate (Sigma-Aldrich), containing 1 mM levamisole as an endogenous alkaline phosphatase inhibitor. Sections were counterstained with methyl green and mounted with Kaiser's glycerol jelly.

**Histomorphometric analysis.** Histomorphometric measurements were made using a BIOQUANT Nova Prime image analysis system (BIOQUANT Image Analysis Corp.). The following primary parameters were determined: bone area, bone perimeter, osteoid area, number of osteoblasts, osteoblast perimeter, number of osteoclasts, osteoclast perimeter, and double-calcein-interlabeled width. From the primary data, the structural parameters of bone area (bone area/tissue area), trabecular width, trabecular number, trabecular separation, and osteoblast and osteoclast surface were calculated. All histomorphometric parameters were expressed according to the recommendations of the American Society for Bone and Mineral Research Nomenclature Committee.

**µCT imaging and analysis.** The distal femurs of WT and *Pthrp*<sup>-/-</sup> mice were scanned using a µCT scanner (µCT 40; SCANCO Medical AG), with matrix size 2,048 × 2,048 and isotropic resolution of 5 µm. Three-dimensional trabecular structural parameters in the secondary spongiosa were directly measured as previously described (7); this has advantages over static bone histomorphometry in that it does not assume the presence of an underlying fixed plate or rod-like trabecular structure. Cortical thickness was

expressed as the average thickness of the 3D cortex on the inner and outer cortical surfaces of the specimens. The specimens were measured blindly, without knowledge of the group code.

**BM cell cultures.** Tibiae and femurs of 6-week-old male WT and *Pthrp*<sup>-/-</sup> mice or *Pthrp*<sup>fllox/fllox</sup> and *Pthrp*<sup>fllox/fllox;cre</sup><sup>Coll</sup> mice were removed under aseptic conditions, and BM cells were flushed out with DMEM containing 10% FCS, 50 µg/ml ascorbic acid, 10 mM β-glycerophosphate, and 10<sup>-8</sup> M dexamethasone. Cells were dispersed by repeated pipetting, and a single-cell suspension was achieved by forceful expulsion of the cells through a 22-gauge syringe needle. Total BM cells (10<sup>6</sup>) were cultured in 36-cm<sup>2</sup> petri dishes in 5 ml of the above-mentioned medium, which was changed every 4 days, and cultures were maintained for 18 days. At the end of the culture period, cells were washed with PBS, fixed with PLP fixative, and stained with methyl blue or cytochemically for alkaline phosphatase. After staining, the numbers of total CFU-f and/or CFU-f<sub>ALP</sub> were counted manually or by computer-assisted image analysis.

**Statistical analysis.** Data from image analysis are presented as means ± SEM. Statistical comparisons were made using a 2-way ANOVA, with *P* < 0.05 being considered significant. Comparisons between groups of µCT scan analyses were performed using the Wilcoxon test.

### Acknowledgments

This work was supported by grants from the Canadian Institutes of Health Research (CIHR) and the Canadian Arthritis Network (to A.C. Karaplis and D. Goltzman), the National Cancer Institute of Canada (to D. Goltzman), and the NIH (AR044855, to H.M. Kronenberg). A.C. Karaplis is the recipient of a CIHR Scientist Award.

Received for publication March 2, 2005, and accepted in revised form June 27, 2005.

Address correspondence to: Andrew C. Karaplis, Department of Medicine and Lady Davis Institute for Medical Research, Sir Mortimer B. Davis Jewish General Hospital, 3755 Cote Sainte Catherine Road, Montréal, Québec, Canada H3T 1E2. Phone: (514) 340-8222 ext. 4907; Fax: (514) 340-7573; E-mail: akarapli@ldi.jgh.mcgill.ca.

Dengshun Miao and Bin He contributed equally to this work.

1. Seeman, E. 2003. Reduced bone formation and increased bone resorption: rational targets for the treatment of osteoporosis. *Osteoporos. Int.* **14**(Suppl. 3):S2–S8.
2. Goltzman, D. 2002. Discoveries, drugs and skeletal disorders. *Nat. Rev. Drug Discov.* **1**:784–796.
3. Juppner, H., et al. 1991. A G protein-linked receptor for parathyroid hormone and parathyroid hormone-related peptide. *Science*. **254**:1024–1026.
4. Miao, D., He, B., Karaplis, A.C., and Goltzman, D. 2002. Parathyroid hormone is essential for normal fetal bone formation. *J. Clin. Invest.* **109**:1173–1182. doi:10.1172/JCI200214817.
5. Reeve, J. 1996. PTH: a future role in the management of osteoporosis? [review]. *J. Bone Miner. Res.* **11**:440–445.
6. Hodzman, A.B., et al. 1997. A randomized controlled trial to compare the efficacy of cyclical parathyroid hormone versus cyclical parathyroid hormone and sequential calcitonin to improve bone mass in postmenopausal women with osteoporosis. *J. Clin. Endocrinol. Metab.* **82**:620–628.
7. Jiang, Y., et al. 2003. Recombinant human parathyroid hormone (1-34) [teriparatide] improves both cortical and cancellous bone structure. *J. Bone Miner. Res.* **18**:1932–1941.
8. Neer, R.M., et al. 2001. Effect of parathyroid hor-

9. Black, D.M., et al. 2003. The effects of parathyroid hormone and alendronate alone or in combination in postmenopausal osteoporosis. *N. Engl. J. Med.* **349**:1207–1215.
10. Rosen, C.J. 2004. What's new with PTH in osteoporosis: where are we and where are we headed? [review]. *Trends Endocrinol. Metab.* **15**:229–233.
11. Strewler, G.J., and Nissenson, R.A. 1990. Hypercalcemia in malignancy. *West. J. Med.* **153**:635–640.
12. Wysolmerski, J.J., and Broadus, A.E. 1994. Hypercalcemia of malignancy: the central role of parathyroid hormone-related protein [review]. *Annu. Rev. Med.* **45**:189–200.
13. Grill, V., Rankin, W., and Martin, T.J. 1998. Parathyroid hormone-related protein (PTHrP) and hypercalcaemia. *Eur. J. Cancer*. **34**:222–229.
14. Karaplis, A.C., et al. 1994. Lethal skeletal dysplasia from targeted disruption of the parathyroid hormone-related peptide gene. *Genes Dev.* **8**:277–289.
15. Lanske, B., et al. 1996. PTH/PTHrP receptor in early development and Indian hedgehog-regulated bone growth. *Science*. **273**:663–666.
16. Jobert, A.S., et al. 1998. Absence of functional receptors for parathyroid hormone and parathy-

17. Karaplis, A.C., et al. 1998. Inactivating mutation in the human parathyroid hormone receptor type 1 gene in Blomstrand chondrodysplasia. *Endocrinology*. **139**:5255–5258.
18. Abou-Samra, A.B., et al. 1992. Expression cloning of a common receptor for parathyroid hormone and parathyroid hormone-related peptide from rat osteoblast-like cells: a single receptor stimulates intracellular accumulation of both cAMP and inositol trisphosphates and increases intracellular free calcium. *Proc. Natl. Acad. Sci. U. S. A.* **89**:2732–2736.
19. Amizuka, N., Warshawsky, H., Henderson, J.E., Goltzman, D., and Karaplis, A.C. 1994. Parathyroid hormone-related peptide-depleted mice show abnormal epiphyseal cartilage development and altered endochondral bone formation. *J. Cell Biol.* **126**:1611–1623.
20. Amizuka, N., et al. 1996. Haploinsufficiency of parathyroid hormone-related peptide (PTHrP) results in abnormal postnatal bone development. *Dev. Biol.* **175**:166–176.
21. Walsh, C.A., et al. 1995. Expression and secretion of parathyroid hormone-related protein by human bone-derived cells in vitro: effects of glucocorticoids. *J. Bone Miner. Res.* **10**:17–25.



22. Kartsogiannis, V., et al. 1997. Temporal expression of PTHrP during endochondral bone formation in mouse and intramembranous bone formation in an in vivo rabbit model. *Bone*. **21**:385–392.
23. Miao, D., et al. 2004. Skeletal abnormalities in Pth-null mice are influenced by dietary calcium. *Endocrinology*. **145**:2046–2053.
24. Miao, D., et al. 2004. Parathyroid hormone-related peptide is required for increased trabecular bone volume in parathyroid hormone-null mice. *Endocrinology*. **145**:3554–3562.
25. Horwitz, M.J., Tedesco, M.B., Gundberg, C., Garcia-Ocana, A., and Stewart, A.F. 2003. Short-term, high-dose parathyroid hormone-related protein as a skeletal anabolic agent for the treatment of postmenopausal osteoporosis. *J. Clin. Endocrinol. Metab.* **88**:569–575.
26. Wysolmerski, J.J., et al. 1998. Rescue of the parathyroid hormone-related protein knockout mouse demonstrates that parathyroid hormone-related protein is essential for mammary gland development. *Development*. **125**:1285–1294.
27. He, B., et al. 2001. Tissue-specific targeting of the pthrp gene: the generation of mice with floxed alleles. *Endocrinology*. **142**:2070–2077.
28. Owen, M., and Friedenstein, A.J. 1988. Stromal stem cells: marrow-derived osteogenic precursors [review]. *Ciba Found. Symp.* **136**:42–60.
29. Chan, G.K., Deckerbaum, R.A., Bolivar, I., Goltzman, D., and Karaplis, A.C. 2001. PTHrP inhibits adipocyte differentiation by down-regulating PPAR gamma activity via a MAPK-dependent pathway. *Endocrinology*. **142**:4900–4909.
30. Chan, G.K., et al. 2003. Parathyroid hormone-related peptide interacts with bone morphogenetic protein 2 to increase osteoblastogenesis and decrease adipogenesis in pluripotent C3H10T 1/2 mesenchymal cells. *Endocrinology*. **144**:5511–5520.
31. Henderson, J.E., et al. 1995. Nucleolar localization of parathyroid hormone-related peptide enhances survival of chondrocytes under conditions that promote apoptotic cell death. *Mol. Cell. Biol.* **15**:4064–4075.
32. Amling, M., et al. 1997. Bcl-2 lies downstream of parathyroid hormone-related peptide in a signaling pathway that regulates chondrocyte maturation during skeletal development. *J. Cell Biol.* **136**:205–213.
33. Dougherty, K.M., et al. 1999. Parathyroid hormone-related protein as a growth regulator of prostate carcinoma. *Cancer Res.* **59**:6015–6022.
34. Tovar Sepulveda, V.A., Shen, X., and Falzon, M. 2002. Intracrine PTHrP protects against serum starvation-induced apoptosis and regulates the cell cycle in MCF-7 breast cancer cells. *Endocrinology*. **143**:596–606.
35. Schorr, K., Taimor, G., Degenhardt, H., Weber, K., and Schluter, K.D. 2003. Parathyroid hormone-related peptide is induced by stimulation of alpha 1A-adrenoceptors and improves resistance against apoptosis in coronary endothelial cells. *Mol. Pharmacol.* **63**:111–118.
36. Hastings, R.H., et al. 2003. Parathyroid hormone-related protein ameliorates death receptor-mediated apoptosis in lung cancer cells. *Am. J. Physiol. Cell Physiol.* **285**:C1429–C1436.
37. Massfelder, T., et al. 2004. Parathyroid hormone-related protein is an essential growth factor for human clear cell renal carcinoma and a target for the von Hippel-Lindau tumor suppressor gene. *Cancer Res.* **64**:180–188.
38. Aarts, M.M., et al. 1999. Parathyroid hormone-related protein interacts with RNA. *J. Biol. Chem.* **274**:4832–4838.
39. Tazawa, H., Takahashi, S., and Zilliacus, J. 2003. Interaction of the parathyroid hormone receptor with the 14-3-3 protein. *Biochim. Biophys. Acta*. **1620**:32–38.
40. Suda, T., et al. 1999. Modulation of osteoclast differentiation and function by the new members of the tumor necrosis factor receptor and ligand families. *Endocr. Rev.* **20**:345–357.
41. Du, P., Seitz, P.K., and Cooper, C.W. 2000. Regulation of PTH/PTH-related protein receptor expression by endogenous PTH-related protein in the rat osteosarcoma cell line ROS 17/2.8. *Endocrine*. **12**:25–33.
42. Vilardaga, J.P., et al. 2002. Internalization determinants of the parathyroid hormone receptor differentially regulate beta-arrestin/receptor association. *J. Biol. Chem.* **277**:8121–8129.
43. Spurney, R.F., et al. 2002. Anabolic effects of a G protein-coupled receptor kinase inhibitor expressed in osteoblasts. *J. Clin. Invest.* **109**:1361–1371. doi:10.1172/JCI200214663.
44. Miyakoshi, N., Kasukawa, Y., Linkhart, T.A., Baylink, D.J., and Mohan, S. 2001. Evidence that anabolic effects of PTH on bone require IGF-I in growing mice. *Endocrinology*. **142**:4349–4356.
45. Bikle, D.D., et al. 2002. Insulin-like growth factor I is required for the anabolic actions of parathyroid hormone on mouse bone. *J. Bone Miner. Res.* **17**:1570–1578.
46. Hurley, M.M., et al. 1999. Parathyroid hormone regulates the expression of fibroblast growth factor-2 mRNA and fibroblast growth factor receptor mRNA in osteoblastic cells. *J. Bone Miner. Res.* **14**:776–783.
47. Hurley, M.M., Yao, W., Arnaud, C.D., and Lane, N.E. 2004. hPTH (1-34) treatment increased serum FGF2 levels in glucocorticoid induced osteoporosis patients. *J. Bone Miner. Res.* **19**:S459.
48. Miao, D., and Scutt, A. 2002. Histochemical localization of alkaline phosphatase activity in decalcified bone and cartilage. *J. Histochem. Cytochem.* **50**:333–340.